Chemical Engineering Journal 385 (2020) 123923

Contents lists available at ScienceDirect

Chemical Engineering Journal

journal homepage: www.elsevier.com/locate/cej

Mechanistic inference on the reaction kinetics of phenols and anilines in carbon nanotubes-activated peroxydisulfate systems: pp-LFERs and QSARs analyses

Hanrui Su[a], Yan Wei[a], Xiaolei Qu[b], Chunyang Yu[c], Qilin Li[d], Pedro J.J. Alvarez[d], Mingce Long[a,*]

[a] School of Environmental Science and Engineering, Key Laboratory for Thin Film and Microfabrication of the Ministry of Education, Shanghai Jiao Tong University, Shanghai 200240, China
[b] State Key Laboratory of Pollution Control and Resource Reuse, School of the Environment, Nanjing University, Jiangsu 210023, China
[c] School of Chemistry and Chemical Engineering, Shanghai Jiao Tong University, Shanghai 200240, China
[d] Department of Civil and Environmental Engineering, Rice University, Houston, TX 77005, United States

HIGHLIGHTS

- Carbon nanotubes (CNTs) activate PDS following Langmuir–Hinshelwood kinetics.
- QSAR/pp-LFER models for CNTs/PDS oxidation of phenols and anilines were developed.
- The surface affinities mainly depend on π-π and hydrophobic interactions.
- Single-electron transfer ability is a key rate predictor in CNTs/PDS systems.

GRAPHICAL ABSTRACT

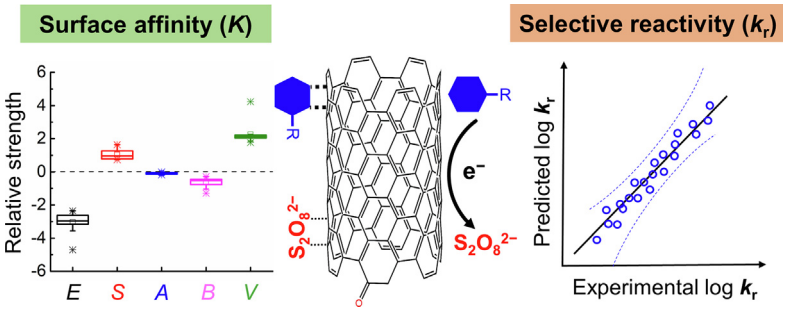

ARTICLE INFO

Keywords:
Persulfate activation
Carbon nanotubes
Non-radical oxidation
Quantitative structure-activity relationships
Polyparameter linear free energy relationships

ABSTRACT

There is increasing interest in persulfate (peroxydisulfate (PDS) and peroxymonosulfate (PMS)) activation by (non-toxic) metal-free catalysts for advanced oxidation of organic contaminants. Nevertheless, the non-radical reaction mechanisms of these catalytic reactions are not well understood. Herein, we provide mechanistic inference on the non-radical reaction pathway of the carbon nanotubes (CNTs)/persulfate system and the associated kinetics. We determined the initial degradation rates of 18 phenols and 4 anilines at various initial concentrations by commercial multiwalled carbon nanotubes (MWCNTs) and peroxydisulfate (PDS), which followed binary Langmuir–Hinshelwood kinetics. Polyparameter linear free energy relationships (pp-LFERs) and quantitative structure-activity relationships (QSARs) were developed for the equilibrium adsorption constant (K) and the surface reaction rate constant (k_r). QSAR analyses for log$K$ suggested that affinity interactions between organics and MWCNTs are mainly related to π-π interactions. The molecular volume term (V) in the pp-LEFRs contributes the most to the interaction, indicating hydrophobic interactions are also significant. QSAR analyses for log k_r indicated one-electron oxidation potential (E_{ox}, representing single-electron transfer ability) and polarizability (α) are predominant factors affecting the reactivity of aromatic organics towards MWCNTs/PDS. Additionally, non-radical reactions occur between adsorbed aromatic compounds and adsorbed PDS, indicating that surface interactions and reactions with MWCNTs dominate the overall reaction rates.

* Corresponding author.
E-mail address: long_mc@sjtu.edu.cn (M. Long).

https://doi.org/10.1016/j.cej.2019.123923
Received 2 September 2019; Received in revised form 27 November 2019; Accepted 22 December 2019
Available online 24 December 2019

1. Introduction

Non-radical oxidative processes in persulfate (peroxydisulfate (PDS) or peroxymonosulfate (PMS)) activation have drawn increasing attention for the removal of refractory organic contaminants from water. These non-radical processes usually exhibit a milder oxidative power than free radicals. However, they have significant advantages over radicals-based advanced oxidation processes, such as avoiding significant scavenging by abundant inorganic ions (e.g., salts) and natural organic matter, and preventing formation of toxic halogenated byproducts [1]. Therefore, non-radical oxidative processes may be ideal for pre-treatment of toxic wastewaters and for selective removal of trace hazardous organics in complex water matrices or high-salinity waters [1,2]. Among the broad range of catalysts for persulfate activation through non-radical pathways, metal-free carbocatalysts are attractive because they avoid the inherent drawback of secondary pollution from metal-based catalysts [2]. Whereas some concerns about health effects of carbocatalysts (e.g., CNTs) have been raised [3], several processes in natural environments such as aggregation, precipitation, sorption, and biotransformation significantly decrease their bioavailability and cytotoxicity, mitigating potential associated risks [4–6].

Carbonaceous materials such as reduced graphene oxide (rGO) [7], carbon nanotubes (CNTs) [8], nanodiamonds [9], activated carbon [10], or other nanocarbons [11,12] have been extensively investigated as metal-free catalysts. Among these, CNTs showed high activation abilities for both PMS and PDS [8,13]. The prevailing view of the non-radical mechanism for PMS/PDS activation involves: (1) formation of surface activated PMS/PDS complex that could effectively react with the electron-rich organic contaminants [14–17]; (2) CNTs also act as mediators to facilitate electron transfer directly from organic contaminants to PMS/PDS [18,19]; and (3) singlet oxygen ($^1O_2$) is generated from ketonic groups on the surface of CNTs [20] to subsequently oxidize organics. Although these prior studies have advanced understanding of non-radical mechanisms, critical knowledge gaps remain on several important aspects, including (1) accurate assessment of interactions between the substrates and catalyst surfaces, (2) understanding the molecular structure dependent oxidation process, and (3) quantitative prediction of selective oxidation rates for specific organic contaminants.

The substrate-dependent reactivity is the basis for the selective nature of the non-radical pathways in persulfate activation. Lee et al. found that nitrobenzene and benzoic acid were more resistant to degradation compared to phenolic compounds [15]. Guan et al. found that the reaction rates of phenols correlate well with their Hammett constant σ^+ and half-wave oxidation potential ($E_{1/2}$) [17]. Our recent work suggests that the selectivity in the removal of aromatic compounds (ACs) depends strongly on the ionization potential (IP) of the organics [12]. Studying the substrate-dependent oxidation capacity is important to predict the treatability of organic contaminants and explore the non-radical mechanism in the persulfate activation processes. However, previous studies did not systematically investigate the specific contributions of factors affecting the substrate-dependent interactions as well as the reactivity of ACs in persulfate activation. Quantitative structure-activity relationships (QSARs) are powerful approaches to correlate response variables and a set of descriptors of molecules, which has been used to predict reaction rate constants for organic contaminants oxidation in various systems [21–23]. Accordingly, polyparameter linear free energy relationships (pp-LFERs) present robust and accurate methods for understanding and prediction of partitioning processes, including sorption of chemicals on carbonaceous sorbents [24–26].

To predict surface affinity and reaction rates, the kinetic model should consider the multi-step non-radical reactions of organic contaminants in CNTs/persulfate systems. Several kinetic models such as Langmuir-Hinshelwood (L-H) [20,27], Eley-Rideal [28], and Michaelis–Menten [29,30] have been used to describe heterogeneous catalytic processes based on mechanisms that are not radical-mediated. Among these, L-H model is the most commonly used kinetic expression based on the assumption that surface degradation follows adsorption of both reactants to the catalyst surface. Thus, this model could potentially be used as a basis to describe the CNTs/persulfate systems.

To address the knowledge gaps identified above, we develop an L-H kinetic model to discern the multiple processes in PDS activation and organic degradation over multiwalled CNTs (MWCNTs). The apparent equilibrium adsorption constants and reaction rate constants were determined for 18 phenols and 4 anilines at different concentrations. Then, QSARs were established to predict the substrate-dependent selectivity of various ACs and characterize the influence of structural characteristics (e.g., substituents and quantum chemical properties). While the pp-LFER models using Abraham descriptors were established particularly to characterize just the interaction between substrate and CNTs. Finally, a specific non-radical mechanism was proposed for ACs oxidation by the CNTs/persulfate system, which enables predictions of preferential interactions and treatability of specific organics in water.

2. Material and methods

2.1. Chemicals

Commercial MWCNTs (> 95% purity) with a length of 50 μm were obtained from Chengdu Organic Chemicals Co., Ltd. Transmission electron microscopy (TEM; G2F20, TECNAI) revealed that the diameters of MWCNTs were about 10–20 nm (Fig. S1). The MWCNTs were treated with 3 M aqueous HCl solution for 24 h to remove impurities [18]. All standards for the phenolic and aniline compounds, $K_2S_2O_8$, NaH_2PO_4, and Na_2HPO_4 were analytical grade and purchased from Sinopharm Chemical Reagent Co., Ltd. To avoid the appearance of ionic species, no organic acids were considered, and the stock solutions of all tested ACs (phenols and anilines) were prepared with a 1×10^{-2} M phosphate buffer solution (PBS, pH = 6.0). Methanol of high-performance liquid chromatography (HPLC) grade was obtained from Thermo Fisher Scientific Co. Ltd.

2.2. Kinetic experiments

Batch kinetic experiments were conducted according to the following procedure. Each experiment was performed using a 50 mL reaction solution in PBS (1×10^{-2} M, pH = 6.0) containing a standard aromatic compound (0.02–0.4 mM) and MWCNTs catalysts (0.1 g/L) kept in a 25 °C water bath. The suspension was continuously agitated using a magnetic stirrer to ensure dispersion. The aggregation status of MWCNTs is expected to be the same in each experiment due to the same reaction conditions. The preliminary experiments demonstrated that PDS alone or PDS in PBS did not result in degradation of ACs (Figs. S2 and S3a). In addition, excessive quenching agents for both sulfate radical ($SO_4^{\cdot -}$) and hydroxyl radical (·OH) (i.e., methanol and ethanol, $n_{\text{quenching agent}}/n_{\text{PDS}}$ = 1000:1) exhibited negligible effects on phenol degradation (Fig. S3b). Further, the adsorption kinetic measurement was conducted to determine adsorption equilibrium time. The results suggest that the adsorption reached equilibrium within 30 min (Fig. S3c). After 30 min adsorption, the oxidation reaction was initiated by adding an aliquot of PDS (1×10^{-3} M). At predetermined intervals, 0.5 mL of sample was withdrawn, immediately filtered and collected in a HPLC vial containing 0.5 mL methanol to terminate the catalytic reaction. The concentrations of ACs were quantitatively determined by HPLC (LC-2010AHT, Shimadzu) equipped with a C-18 column (Shimpack GIST C18) and an UV–vis detector (SPD-20AV). Detailed HPLC operating conditions were listed in Table S1. The reaction intermediates of 4-chlorophenol and 4-chloroaniline were investigated using a Waters Acquity ultra-performance liquid chromatography coupled with a Xevo G2-XS QTof mass spectrometer (UPLC–MS). In addition to the aqueous supernatant samples, the separated MWCNTs were extracted with

methanol to analyze adsorbed polymerized intermediates. All experiments were conducted in triplicate and expressed as means ± standard deviation.

2.3. Kinetic models

The binary L-H kinetic model was expressed as Eq. (1) [27,31]. The values of K, K_p, and k_r were obtained from double-reciprocal plots (Eq. (2)).

$$v = -\frac{d[AC]}{dt} = k_r \frac{K[AC]_0}{1 + K[AC]_0 + K_p[PDS]_0} \quad (1)$$

$$\frac{1}{v} = \frac{1}{k_r K}\frac{1}{[AC]_0} + \frac{1}{k_r} + \frac{K_p[PDS]_0}{k_r K[AC]_0} \quad (2)$$

Here, v (M s^{-1}) is the initial reaction rate, determined from initial kinetics data only at the beginning of the reaction, calculated as changes in concentration divided by reaction time; $[AC]_0$ and $[PDS]_0$ (M) are initial concentrations of aromatic compounds and PDS, respectively; K (M^{-1}) and K_p (M^{-1}) are the respective apparent equilibrium adsorption constant of aromatic compounds and PDS; k_r (M s^{-1}) is the reaction rate constant.

2.4. Molecular descriptors

Fourteen representative molecular descriptors of ACs that known to influence selective reactivity in CNTs/PDS systems [17,19], adsorption affinity for carbon adsorbents [25,32], and oxidation reactivity in other non-radical or radical systems [33–35] were selected to establish quantitative relationships between reaction kinetics parameters and structural properties (Tables S2 and S3). They are the number of hydrogen bond donors (#HD), logarithm octanol water partition coefficients (log P), logarithm aqueous solubility (log S), energy of the highest occupied molecular orbital (E_{HOMO}), energy of the lowest unoccupied molecular orbital (E_{LUMO}), the gap of E_{LUMO} and E_{HOMO} (E_{gap}), ionization potential (IP), electron affinity (EA), electronegativity (χ), dipole moment (μ), average polarizability (α), the most positive net atomic charge on hydrogen atoms (qH^+), one-electron oxidation potential (E_{ox}) and O–H bond dissociation energies (BDE). Merck Molecular Force Field (MMFF94) in the Tinker software (Version 5.1.9) were used for preliminary geometry optimization of ACs [36]. The resulting conformations were further optimized at the density functional theory (DFT) level to search for global minimum structures using the Gaussian 09 W software. The optimized geometry and vibrational frequencies were calculated at B3LYP/6-31 + G(d,p) and M06-2X/6-311 + + G(d,p) levels using the universal solvation model based on solute electron density (SMD) [37,38]. The B3LYP functional is commonly used for quantum chemical descriptors calculations in QSARs [34,37], while the M06-2X functional has been considered appropriate for the studies of kinetics, thermodynamics and electronic properties in single-electron transfer (SET) reactions [38–40]. The SMD model has been successfully applied for simulating water environment [34,38,41]. The net atomic charge values for each compound were obtained based on the natural population analysis (NPA). Other descriptors including physicochemical (#HD, log P, and log S) were obtained from public database (Table S2), and experimental half-wave potentials ($E_{1/2}$) were acquired from the reference (Table S4) [42]. Hammett constants (σ, σ^+, and σ^-) were also considered for quantitatively examining the substituent effects of phenols and anilines (Table S4) [21,43]. Multiple linear regression (MLR) is one of the most transparent methods for the development of QSARs by the Organization for Economic Co-operation and Development (OECD) guidelines. We assumed that log K or log k_r values would be predicted as a linear and additive combination of several descriptors of ACs as has been previously reported [22,23]. A stepwise MLR was used to construct the QSAR models.

2.5. PP-LFERs analyses

pp-LFERs have been widely developed to describe the interaction between solutes and solvent in various phases (Eq. (3)) [24,44–46].

$$\log k = eE + sS + aA + bB + vV + c \quad (3)$$

Wherein, log k is the logarithmic free-energy related property on the processes within two condensed phases (i.e., log K in this study). Abraham descriptors include E, S, A, B, and V, in which E is the excessive molar refraction; S is the polarity/polarizability parameter; A is the hydrogen bond acidity parameter; B is the hydrogen bond basicity parameter; and V is the McGowan volume. The fitting coefficients e, s, a, b, and v, and intercept c were derived from multiple linear regressions. The Abraham descriptor values were obtained from the UFZ-LSER database (https://www.ufz.de/index.php?en=31698) (Table S5) [24]. Statistical parameters such as coefficients of determination (R^2), adjusted coefficients of determination (R^2_{adj}), root-mean-square error ($RMSE$), variance inflation factor (VIF), leave-one-out method (Q^2_{LOO}), and average absolute model bias (AMB) were used for validation of QSAR and pp-LFER models (Table S6) [22,26]. The possibilities of chance correlation between selected descriptors and kinetic parameters were investigated by Y-Scrambling and the values of averaged R^2 scrambled (R^2_{ys}) were reported [47]. The applicability domain was characterized by a Williams plot (i.e., the standardized residuals vs. leverage) (Table S6). Statistical analyses were performed using the IBM SPSS Statistics software (Version 24).

3. Results and discussion

3.1. Kinetic analyses

To analyze the oxidation kinetics of phenol in MWCNTs/PDS systems, we investigated the initial reaction rates at various concentrations of phenol and PDS (Fig. 1a, b). A typical saturation kinetics curve was observed for phenol degradation, in which the initial rates of phenol removal increased rapidly with increasing phenol or PDS concentration at relative lower concentrations, and then approached a plateau at higher phenol or PDS concentrations. The results showed that the oxidation kinetics of ACs by MWCNTs/PDS followed mixed-order kinetics under a wide range of phenol or PDS concentrations, and were limited by the active sites on MWCNTs at high adsorbate concentrations, which were in accordance with the binary L-H kinetic model (Eq. (1)). The R^2 values were 0.987 and 0.996 for $1/v$ vs. $1/[phenol]_0$ and $1/v$ vs. $1/[PDS]_0$, respectively, indicating that Eq. (1) describes well the degradation kinetics of phenol by MWCNTs/PDS. The values of K, K_p, and k_r are 4.06 ± 0.07 × 10^4 M^{-1}, 8.93 ± 0.24 × 10^3 M^{-1}, and 7.34 ± 0.09 × 10^{-8} M^{-1} s^{-1}, respectively. That K is four-fold greater than K_p suggests the affinity of PDS to MWCNTs is lower than that of phenol. Similar results were also found in MWCNT/PMS systems (Fig. S4, Text S1). Saturation kinetics were also observed for phenols or iodide oxidation by CNTs/persulfate, indicating that the number of active sites on the MWCNT surface is limited and thus restricts the overall catalytic processes [16,17,20].

To further investigate the catalytic mechanisms of MWCNTs/PDS, we measured the initial reaction rates at a fixed concentration of phenol versus varying concentration of PDS and vice versa (Fig. 1c, d). The k_r value (k_r = 1/[intercept]) increased with increasing PDS concentration, while K value (K = [intercept]/[slope]) remained almost unchanged (Fig. 1c). The excessive PDS showed non-competitive inhibition kinetics for phenol degradation, in which PDS did not interfere with the adsorption affinity of phenol to MWCNTs. However, excessive phenol hindered the interactions between PDS and MWCNTs, in which K_p decreased as the phenol concentration increased (Fig. 1d). The results agree with higher values of K than K_p, i.e., phenol exhibits higher affinity than PDS to the MWCNTs surface. It indicates that the interactions between MWCNTs surface and ACs or PDS dominated the

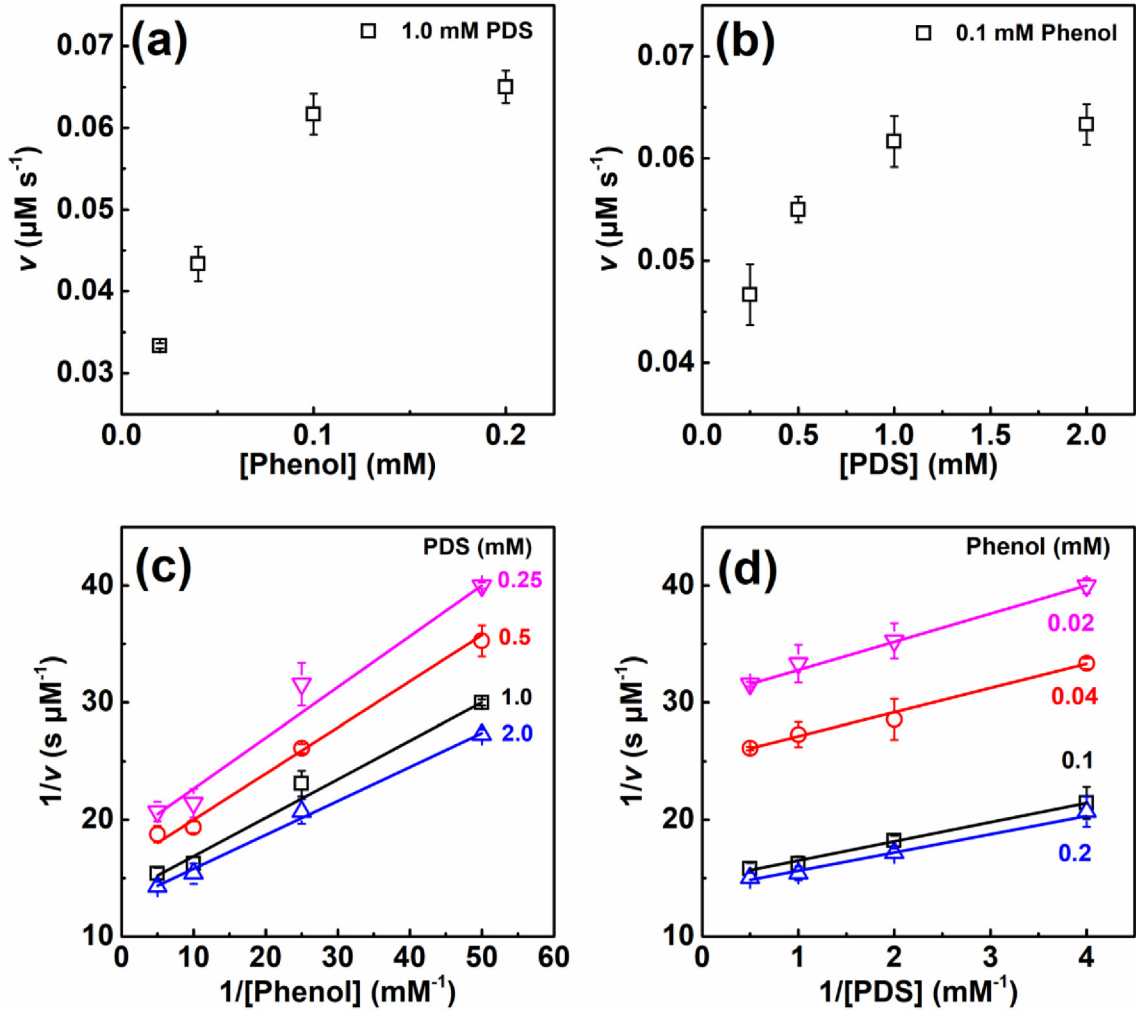

Fig. 1. (a, b) Initial rates of varying concentration of phenol with 1.0 mM PDS and varying concentration of PDS with 0.1 mM phenol. (c, d) Double-reciprocal plots at a fixed concentration of one substrate versus varying concentration of the second substrate for phenol and PDS. Symbols represent measured data and solid lines represent the model fitting. All experiments were performed using 0.1 g/L MWCNTs in 10 mM PBS (pH 6.0) at 25 °C.

catalytic reaction.

At fixed concentrations of PDS and MWCNTs, initial reaction rates at different concentrations of phenols (Fig. S5) and anilines (Fig. S6) were obtained to calculate K and k_r according to Eq. (2). The fitting results of K and k_r values and their log values are summarized in Table 1. The apparent K values are in the range of 0.30–6.03 × 10^4 M^{-1} with a mean value of 2.17 × 10^4 M^{-1}, similar to those reported for phenols and anilines in previous studies [48,49]. The k_r values range widely from 7.6 × 10^{-9} to 1.4 × 10^{-6} M s^{-1}, which are comparable to those reported for other persulfate activation systems [50,51] and ·OH based systems [52]. The half-life ($t_{1/2}$) values of ACs based on the pseudo-first-order kinetic model ($\ln([AC]_0/[AC]_t) = k_{obs} \times t$, $[AC]_0$ = 0.1 mM) were also determined to assess the time scale of degradation (Table S7).

3.2. QSARs for log K

The equilibrium adsorption constant K is generally considered as an indicator of the catalyst's binding affinity for the substrate, representing the strength of interactions between the catalyst and the substrate [50,52–54]. Our data show that MWCNTs possess a high affinity towards ACs as indicated by the high K values, consistent with the observation that the maximum reaction rate was achieved at a relatively low concentration. To better understand the surface interaction mechanisms of ACs in the MWCNTs/PDS system, we developed QSARs relating log K with various descriptors by stepwise MLR (Eq. (4) and Fig. 2a).

$$\log K = 0.42(\pm 1.00) - 0.56(\pm 0.12) \times E_{HOMO}(M06-2X) - 0.33(\pm 0.11) \times \#HD \quad (4)$$

n = 22, R^2 = 0.752, R^2_{adj} = 0.726, $RMSE$ = 0.204, VIF < 1.4, Q^2_{LOO} = 0.700, R^2_{ys} = 0.09, AMB = 1.002.

The values of R^2_{adj} (> 0.6), VIF (< 10) and Q^2_{LOO} (> 0.5) meet the minimum statistical robustness criteria, indicating the model is reasonable for mechanic interpretation [55]. The relatively low value of R^2_{ys} indicates the model is well-founded (not by chance). The applicability domain of QSARs was evaluated by Williams plot (Fig. S7a), which covered all the tested ACs. The negative coefficient with E_{HOMO} (Eq. (4)) suggests that ACs (electron acceptors) with higher electron density (higher value of E_{HOMO}) have weaker π-π electron-donor-acceptor (EDA) interactions with the π clouds on the surface aromatic rings (electron donors) of MWCNTs [56]. The π-π EDA interactions may be enhanced by electron-withdrawing groups (with positive σ^+) that decrease the electrostatic repulsion from the π-system of the interacting ring (Fig. 2b) [56,57]. However, the 95% predictive intervals are relatively wide due to several outliers, which could not be accurately represented by single descriptor σ^+ (Fig. 2b). It is obvious to see that anilines with the same substituents as phenols exhibit lower affinities

Table 1
Apparent equilibrium adsorption constant (K) and reaction rate constants (k_r) of 22 aromatic compounds.

No.	Aromatic compounds	K ($\times 10^4$ M^{-1})	log K	k_r ($\times 10^{-8}$ M s^{-1})	log k_r
1	Phenol	4.06 ± 0.07	4.609	7.34 ± 0.09	−7.134
2	Catechol	0.53 ± 0.07	3.728	31.3 ± 2.42	−6.505
3	Hydroquinone	0.56 ± 0.30	3.750	23.7 ± 0.93	−6.625
4	2-Methylphenol	2.46 ± 0.04	4.391	6.61 ± 0.13	−7.180
5	4-Methylphenol	2.57 ± 0.07	4.411	7.94 ± 0.11	−7.100
6	2-Methoxyphenol	2.35 ± 0.01	4.370	11.2 ± 0.21	−6.953
7	4-Methoxyphenol	2.37 ± 0.11	4.375	12.0 ± 1.11	−6.922
8	4-Acetamidophenol	0.75 ± 0.18	3.875	20.1 ± 0.84	−6.697
9	2-Nitrophenol	2.17 ± 0.16	4.337	2.10 ± 0.38	−7.678
10	4-Nitrophenol	4.86 ± 1.43	4.686	0.76 ± 0.00	−8.117
11	2-Chlorophenol	3.16 ± 0.11	4.499	7.69 ± 1.24	−7.114
12	4-Chlorophenol	3.30 ± 0.04	4.518	7.01 ± 0.10	−7.155
13	2-Bromophenol	1.62 ± 0.34	4.209	9.79 ± 1.26	−7.009
14	4-Bromophenol	2.05 ± 0.04	4.312	7.18 ± 0.24	−7.144
15	2-Hydroxybenzaldehyde	6.03 ± 0.35	4.780	2.06 ± 0.12	−7.686
16	4-Hydroxybenzaldehyde	3.45 ± 0.06	4.538	1.70 ± 0.16	−7.770
17	4,4′-Biphenol	0.36 ± 0.02	3.558	8.14 ± 0.75	−7.090
18	Bisphenol A	1.45 ± 0.09	4.163	5.42 ± 0.17	−7.266
19	Aniline	0.30 ± 0.03	3.478	30.42 ± 0.21	−6.517
20	4-Hydroxyaniline	0.35 ± 0.03	3.544	139 ± 7.05	−5.857
21	4-Nitroaniline	2.15 ± 0.29	4.333	1.42 ± 0.18	−7.846
22	4-Chloroaniline	0.92 ± 0.06	3.962	27.11 ± 1.63	−6.567

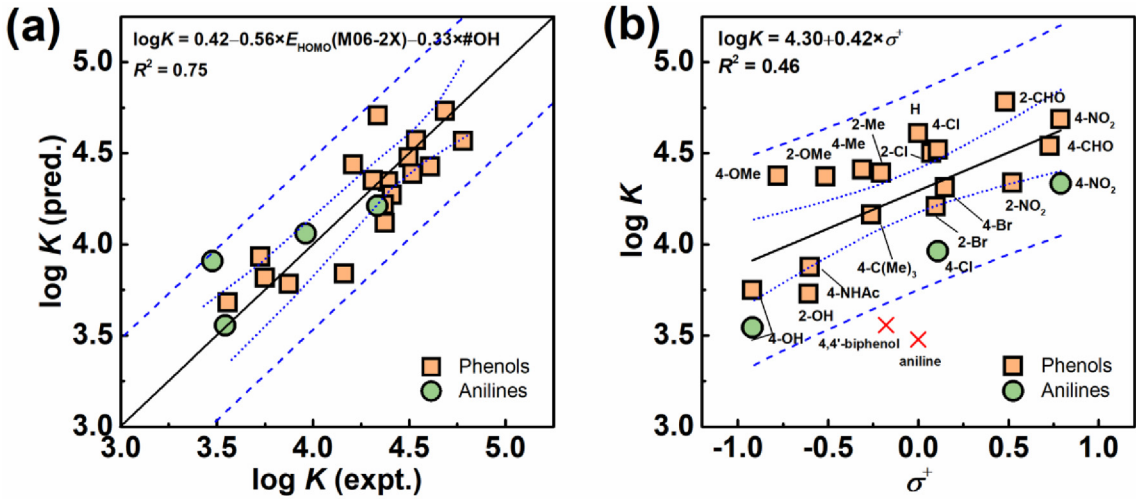

Fig. 2. (a) Plots of the measured and predicted log K for phenolic and aniline compounds based on QSAR model. (b) Correlations between measured log K and Hammett σ^+. The dot and dash lines represented the 95% confidence interval and 95% predictive interval, respectively. Red crosses were outliers. (For interpretation of the references to colour in this figure legend, the reader is referred to the web version of this article.)

towards MWCNTs, which can also be explained by the π-π EDA interactions. The electron-donating ability of amino group (–NH_2) is stronger than that of hydroxyl group (–OH), making the benzene rings electron-rich and thus weakening the interaction with CNTs [49].

The number of hydrogen bond donors (#HD), related to the hydrogen bond donating ability of a molecule, is also included in QSAR models for predicting the affinity (log K) between MWCNTs and ACs. However, the negative sign shows that ACs with more hydrogen bond donors (e.g., catechol, hydroquinone and 4-hydroxyaniline) possess lower affinities toward MWCNTs. This suggests that H-bonding interaction with benzene rings or residual ketonic groups in MWCNTs is not the primary interaction mechanism between ACs and MWCNTs [58]. One possible reason is that ACs with more hydrogen bond donors also have more electron-donating substituted groups (e.g., –OH and –NH_2); they hinder the π-π EDA interaction with MWCNTs as π-electron-donors [25,58]. Hence, π-π EDA bonds other than hydrogen bonds may play a vital role in the interactions of the tested ACs with MWCNTs.

3.3. pp-LFERs for log K

In order to identify the specific interactions between ACs and MWCNTs in the non-radical persulfate activation, pp-LFERs were established for the apparent equilibrium adsorption constants K. There is a significant correlation between log K and the Abraham descriptors (Fig. 3a and Eq. (5)).

$$\log K = -2.923E + 0.857S - 0.159A - 1.423B + 2.272V + 4.675 \quad (5)$$

$n = 22$, $R^2 = 0.755$, $R^2_{adj} = 0.679$, $RMSE = 0.221$, VIF < 6.4, $Q^2_{LOO} = 0.623$, $R^2_{ys} = 0.25$, AMB = 1.002.

The R^2 value of pp-LFERs is slightly better than QSAR model. The VIF values are less than 10, indicating no potential collinearities among the descriptors included in the models. Further, all tested phenols and anilines are lying within the applicability domain (Fig. S7b). Consequently, pp-LFER models can be used to predict K values reflected adsorption affinities of phenolic and aniline compounds on MWCNTs.

The values of each term (represented by multiplication of the correlation coefficient and the Abraham descriptor; i.e., eE, sS, aA, bB and

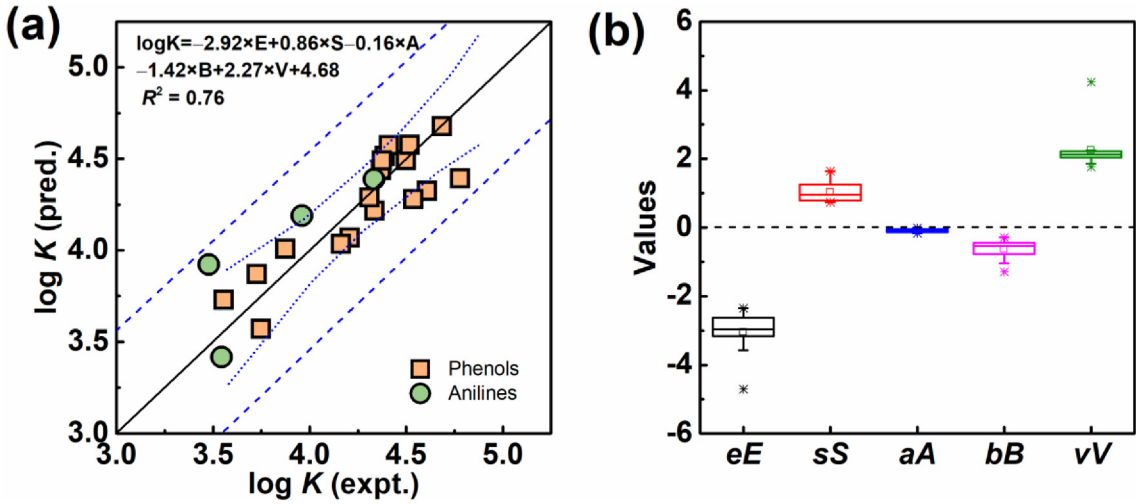

Fig. 3. (a) Measured versus predicted log *K* for phenolic and aniline compounds based on pp-LFERs model. The dot and dash lines represented the 95% confidence interval and 95% predictive interval, respectively. (b) Box and whisker plots for the values of different interaction terms in PP-LFERs model.

vV) for each compound are shown in Fig. 3b, which represents the total contributions of these interaction terms to log *K*. The term *vV* has the most positive contributions (ranging from 26% to 36%), determining the dispersion interactions and the hydrophobic interactions that are involved in the energy requirement for cavity formation. Similarly, previous studies found that the aqueous adsorption energies of some aliphatic and aromatic organic pollutants on carbon nanomaterials including CNTs were mainly determined by nonspecific and hydrophobic interactions (*vV*) [26,59,60]. The term *sS*, describing the specific electrostatic interactions related to polarity and polarizability, contributes positively (11–20% of the total interactions) to log *K*. This indicates that these ACs have strong dipole-dipole and dipole-induced dipole interactions with MWCNTs. The negative contribution of *eE* to the total interaction is in the range of 37–47%. The term *E* is associated with induction effects (i.e., π and n-electron pair interactions), indicating the π-electrons or n-electrons (electrons in the outermost orbital of an atom that do not bond with other atoms) of ACs exist weaker interactions with π electrons of MWCNTs than water molecules. Hydrogen bonding interactions represented by hydrogen bond acidity (*aA*) and hydrogen bond basicity (*bB*) have small contributions (6–17% of the total interactions, respectively) to the log *K* value. The less influential role of *aA* and *bB* may be attributed to the competition of water against ACs for interacting with MWCNTs [26,60]. Previous pp-LFERs studies conducted for activated carbon, SWCNTs and MWCNTs also reported statistically insignificant contribution of the *A* or *B* term to adsorption of aromatic contaminants [26,60,61]. The same studies also found insignificant contributions from the *S* and *E* terms, which is different from our analysis. This may be attributed to the difference in the adsorbents as well as the number and types of organic compounds tested. Note that the nature of π-π interactions has been well established in the association between aromatic compounds and CNTs [25,49,56,58]. Although π-π interactions cannot be fully identified by pp-LFERs, they can be included in the interactions described by the terms *vV*, *sS* and *eE* [26,62]. Therefore, the affinities of the tested ACs to the MWNCTs depend much on their π-π interactions, consistent with that in QSARs (Eq. (4)). Taken together, these QSAR and pp-LFERs models demonstrate that the π-π EDA interactions and hydrophobic interactions prevail between phenols or anilines and MWCNTs.

3.4. QSARs for log k_r

The kinetic parameter k_r is the catalytic reaction rate constant for the adsorbed substrate compound, and correlates well with $t_{1/2}$ derived from the pseudo-first-order kinetics (log k_r vs log $t_{1/2}$, R^2 = 0.96). To systematically analyze the substrate-dependent oxidation capacity of ACs by MWCNTs/PDS, a correlation analysis between the log k_r and selected individual descriptors was performed firstly to access any possible linear relationships. Several descriptors are found to be correlated well with log k_r. The statistically significant ($p < 0.01$) correlations are listed in Table S8, in which the substituent effects (Hammett σ^+ and σ^-), the descriptors related to SET (such as E_{HOMO}, IP, χ and E_{ox}), and hydrogen atom transfer (HAT) ability (BDE) are the possible factors affecting the reactivity of ACs in the MWCNTs/PDS system (Fig. 4). Among the functionals used for calculation, the correlation of descriptors calculated by B3LYP is slightly better than M06-2X, as was previously reported [34].

Hammett constants σ^+ and σ^- inversely correlate well with log k_r, indicating ACs with electron-donating substituents reacted faster with PDS over MWCNTs (Fig. 4a, Eqs. (6) and (7)).

$$\log k_r = -7.14(\pm 0.07) - 0.82(\pm 0.13) \times \sigma^+ (n = 22,\ R^2 = 0.677) \quad (6)$$

$$\log k_r = -6.95(\pm 0.07) - 0.73(\pm 0.11) \times \sigma^- (n = 22,\ R^2 = 0.682) \quad (7)$$

These results are in consistence with prior studies on oxidation of phenols or anilines, which show σ^- (manganese dioxide (MnO_2) [34] and $^1O_2$ [63]) and σ^+ (Ozone (O_3) [21] and hexavalent ferrate (Fe(VI)) [21]) as independent variables. The sensitivity of log k_r to the substituent effect observed in this study is similar to a previous study showing a slope ρ of −1.03 for the correlation [17], but smaller than that reported for MnO_2 or $^1O_2$ oxidation processes [34,63].

In addition to Hammett constants, quantum chemical descriptors also correlate well with log k_r. The general trend illustrated that the log k_r decreases with IP and increases with E_{HOMO} (Fig. 4b, Eqs. (8) and (9)).

$$\log k_r = -1.51(\pm 0.81) - 0.95(\pm 0.14) \times \mathrm{IP(B3LYP)} (n = 22,\ R^2 = 0.704) \quad (8)$$

$$\log k_r = -1.18(\pm 0.81) + 0.97(\pm 0.13) \times E_{HOMO}\mathrm{(B3LYP)} (n = 22,\ R^2 = 0.728) \quad (9)$$

The result suggests that the compound that has a stronger capability to donate an electron (higher E_{HOMO} or lower IP) has a higher reaction rate. Another quantum chemical descriptor E_{gap} has been found as the predominant descriptor affecting oxidation of emerging micropollutants by $SO_4^{\cdot -}$ in water [22]. Nevertheless, a weak correlation (R^2 = 0.253) was found between log k_r and E_{gap}(B3LYP). It indicates that the reactions of MWCNTs/PDS with the ACs are more likely to proceed through a non-radical pathway.

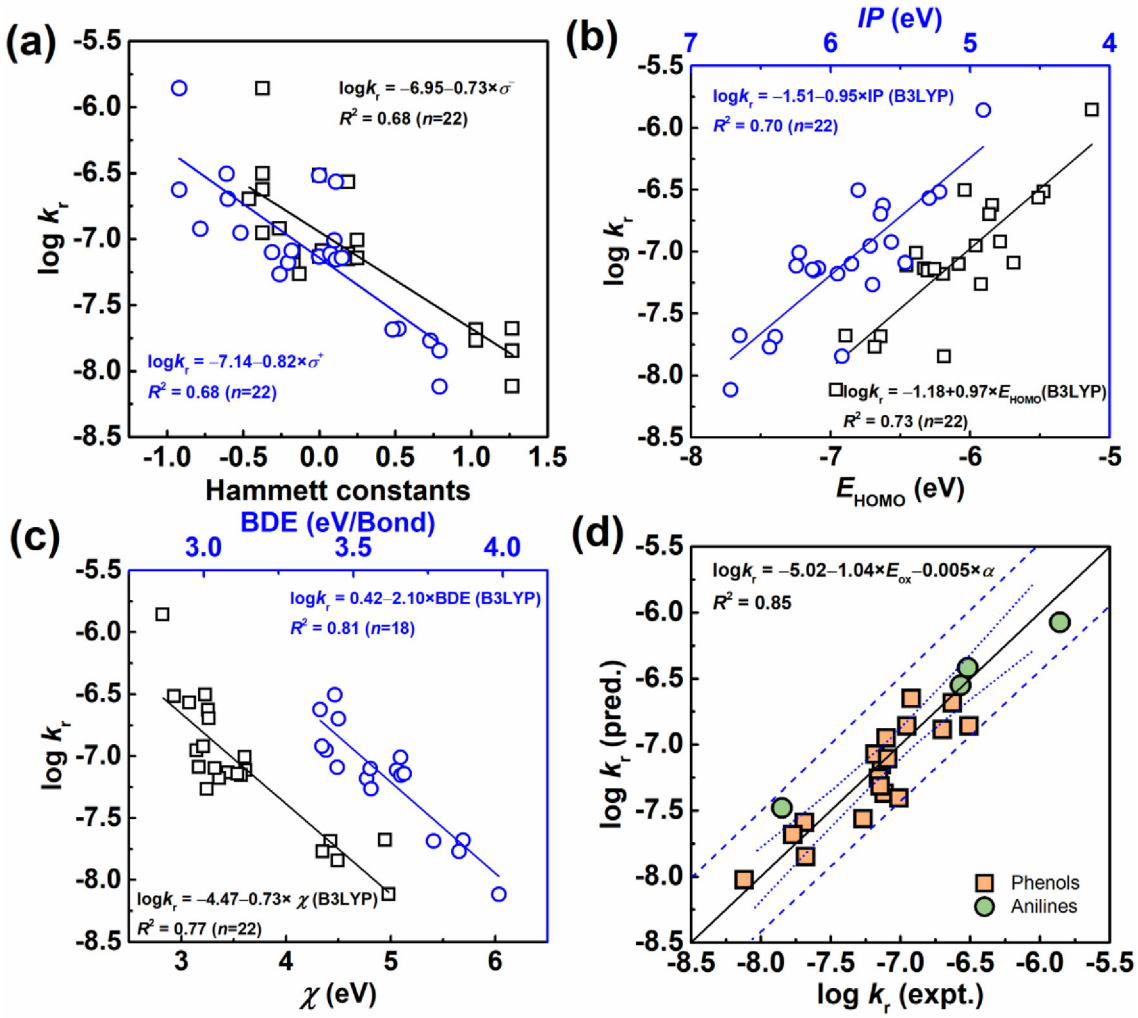

Fig. 4. Correlations between log k_r and (a) Hammett constants (σ^+ and σ^-); (b) E_{HOMO} and IP; (c) χ and BDE for varied aromatic compounds. (d) Plots of the measured and predicted log k_r for phenolic and aniline compounds based on QSAR model.

Among the descriptors that correlated with log k_r, the R^2 for χ is the highest (Fig. 4c, Eq. (10)). The electronegativity is defined as χ = (IP + EA)/2, which represents the tendency to attract electrons. In the case of ACs oxidation by MWCNTs/PDS, the lower the χ value, the higher the rate constants, similar to the ozone oxidative systems [64]. They are different, however, from reported studies on oxidation with · OH, which positively correlated to χ [65]. The discrepancy may be attributed to the difference in the specific mechanisms involved. The · OH being an electrophile tends to attack molecules with higher χ, while PDS could serve as an electron acceptor to abstract electrons from ACs with lower χ. As for phenolic compounds (n = 18), BDE (representing the reaction enthalpy of hydrogen atom splitting-off from the O–H bond of phenolic hydroxyl groups) shows highest correlation with log k_r, indicating that homolytic cleavage of the O–H bond is a crucial process (Fig. 4c, Eq. (11)).

$$\log k_r = -4.47(\pm 0.33) - 0.73(\pm 0.09) \times \chi(\text{B3LYP}) (n = 22,\ R^2 = 0.769) \quad (10)$$

$$\log k_r = 0.42(\pm 0.91) - 2.10(\pm 0.25) \times \text{BDE(B3LYP)} (n = 18,\ R^2 = 0.813) \quad (11)$$

There is no surprise that the descriptors having good correlations with log k_r are significantly cross-correlated, since divergent substituents of ACs would inevitably affect electrostatic and quantum chemical properties of molecules (Table S9). Therefore, these descriptors should be used individually. To avoid missing descriptors with low correlation but high importance, all descriptors (n = 14) were selected for developing QSARs for log k_r using stepwise MLR (Eq. (12) and Fig. 4d).

$$\log k_r = -5.02(\pm 0.23) - 1.04(\pm 0.10) \times E_{ox}(\text{B3LYP}) - 0.005(\pm 0.001) \times \alpha(\text{B3LYP}) \quad (12)$$

n = 22, R^2 = 0.854 R^2_{adj} = 0.838, $RMSE$ = 0.210, VIF < 1.1, Q^2_{LOO} = 0.801, R^2_{ys} = 0.09, AMB = 1.006.

The relatively high R^2_{adj} value and narrow confidence and prediction intervals with AMB = 1.006 indicates that Eq. (12) is mechanistically interpretable and satisfactory for predicting the reactivity of unknown chemicals by MWCNTs/PDS systems. The VIF value (< 10) indicates that the descriptors are not strongly correlated with each other. As can be seen from Fig. S7c, all data points fall into the applicability domain, indicating the QSAR models are broadly applicable to phenolic and aniline compounds. Although 4,4′-biphenol (h = 0.282) and bisphenol A (h = 0.352) have relatively high leverages compared to other ACs presumably due to their higher polarizability resulting from the two aromatic rings, their h values still fall below h^*. The one-electron oxidation potential (E_{ox}) is the most influencing factor on log k_r. The ACs with higher E_{ox} values are relatively difficult to oxidize. For example, 4-nitroaniline (E_{ox} = 1.492 V) shows significantly lower reaction rates than 4-chloroaniline (E_{ox} = 0.839 V). E_{ox} represents the energy required for the half-reaction of one electron loss, revealing that one-

electron oxidation is the rate-limiting step in ACs oxidation, corroborating their oxidation in other non-radical systems (MnO_2 [34], $^1O_2$ [63], and peroxidases [66]). The slope ($\rho = -2.11$, Table S8) of measured half-wave potential ($E_{1/2}$) is also comparable with log k_{rel} of phenols oxidized by MWCNTs/PDS ($\rho = -2.89$) reported previously [17], confirming that one-electron oxidation potentials of ACs determine reaction rates via the SET route. The second important descriptor is α, but only contributes 28.6% of the variance. The average polarizability characterizes the induced dipole moment of a molecule to the electric field, which is related to chemical reactivity [67]. As the polarizability of ACs increase, it was less likely to react in the MWCNTs/PDS system.

3.5. Persulfate activation mechanisms

Results from kinetics analyses and implication of model descriptors reveal essential information on the fundamental mechanisms for molecular interaction as well as simultaneous chemical reactions between ACs and MWCNTs/PDS. The results of L-H kinetic model fitting infer that oxidative degradation of ACs by MWCNTs/PDS occurs through a two-step, non-radical, catalytic mechanism: PDS and ACs adsorb on the surface of CNTs; CNTs subsequently trigger electron transfer that leads to ACs oxidation and PDS reduction. Specifically, an aromatic molecule binds to the surface of CNTs via π-π interactions or hydrophobic interactions, while a PDS molecule adsorbs on CNTs with a stretched O–O bond. Then, the adsorbed aromatic compound donates one electron from its HOMO to an adsorbed PDS molecule via the sp^2 hybridized conductive carbon framework (Fig. 5), leading to the oxidation of the phenol and reduction of the PDS. After the catalytic reaction is completed, the product desorbs from the surface of the CNTs to recover active sites.

In this catalytic process, the reaction rate depends strongly on surface interactions. The differential affinity (K) between ACs and CNTs surface would result in different adsorption abilities [15], which has been shown for other carbonaceous activators such as nitrogen doped rGO [68] and graphitic biochars [69] in persulfate activation. The specific interactions between ACs and the surface of CNTs are well represented by the pp-LFERs model or descriptors E_{HOMO} and #HD. Both the large π-cloud of the benzene ring and the hydrophilic moieties of the aromatic molecules enhance the adsorption and electron transfer of ACs on MWCNTs surface, thus accelerating the catalytic reaction. Consequently, processes that interfere with ACs interaction with the carbocatalyst surface would hinder the oxidation of ACs, resulting in a decline in the catalytic performance. For example, strong interactions between phenolic intermediates with higher surface affinity and the carbocatalysts surface could cause the immanent deactivation of catalysts by competing with the substrate for active sites on the catalyst surface [17,69]. In addition, the strong persulfate-catalyst interactions favor formation of surface active complexes. The complexes can promote electron mediation from co-adsorbed organics to persulfates in a non-radical pathway. More positive charges on the carbocatalyst surface induced by nitrogen doping could enhance the affinity of negatively charged persulfate [14]. However, it has also been shown that extensive carbon oxidation may result in an inactive state of cabocatalysts if no substrate acts as an electron donor [12,16].

The stronger dependency of the apparent reaction rate constant (k_r) on E_{ox} (or χ, IP, and E_{HOMO}) and α of phenols and anilines is in agreement with the SET mechanism to form phenyl or aniline radical cations. The phenolic or aniline compounds would also form phenoxyl or aminophenyl radicals via SET accompanied by simultaneous proton transfer. The primary radicals in various resonance forms serve as the precursors for diverse secondary reactions. This is corroborated by analyses of the reaction intermediates formed in the 4-chlorophenol and 4-chloroaniline degradation systems, which were identified using UPLC–MS. As shown in the chromatograms (Figs. S8 and S9), 4-chlorophenol can be transformed to chlorinated polymeric products (m/z = 219/221 and 253/255) via C–O or C–C coupling of chlorophenol radicals. Furthermore, 4-chloroaniline can generate several dimers and trimers with the molecular ions of m/z = 218/219/221, 220/221/222, 251/253/255, 327/329/330/338, and 359/361/362/372 via C–C, C–N or N–N coupling (Figs. S10 and S11). Their initial transformation pathways are described in Fig. S12 and S13, and more details are provided in Text S2.

Since the quantitative indicators for SET reactions (E_{ox}, χ, IP, and E_{HOMO}) are general molecular descriptors of organic compounds, the role of the SET mechanism can be extrapolated to include the oxidation of aromatic contaminants besides phenolic and aniline compounds. Moreover, Hammett correlations suggest the dependency of SET reactions on substituents. ACs with strong electron-donating functional groups are more easily oxidized by MWNCTs/PDS than those with electron-withdrawing groups, providing qualitative predictions for k_r.

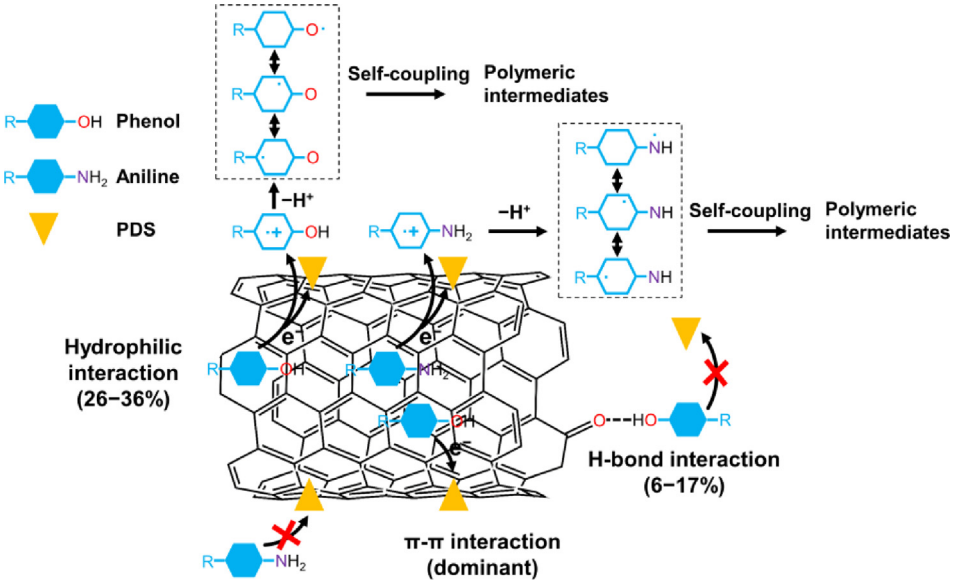

Fig. 5. Proposed reaction mechanisms for PDS activation by MWCNTs.

4. Conclusions

We demonstrated that the oxidation of ACs (18 phenols and 4 anilines) by MWCNTs/PDS followed a binary Langmuir-Hinshelwood kinetics. The kinetic parameters (K and k_r) and a set of 14 molecular descriptors or the 5 Abraham parameters were used to develop QSARs and pp-LFERs to elucidate the selective interactions and oxidations of MWCNTs/PDS-based treatment. The results show that the π-π interactions (mainly) and hydrophobic interactions (26–36%) govern the interactions between ACs and MWCNTs. The k_r values are determined by substituents (Hammett σ^- and σ^+) and the abilities related to single electron transfer (E_{ox}) of ACs. The models developed in this study reveal the nature of the specific interactions between the catalyst and substrate or oxidant as well as the surface reaction mechanisms, filling a critical knowledge gap in our understanding of non-radical mediated advanced oxidation processes especially for persulfate activation. Moreover, the models could be generalized to discern the interactions between reacting species and carbocatalysts in persulfate activation for predicting the substrate-dependent affinity of contaminants with various structures. The present study advances understanding of how the structures of low molecular weight aromatic compounds (MW < 150 g/mol) affect their reactivity in non-radical mediated oxidation processes and enhances the rational selection of persulfate-based oxidative systems. Further efforts could expand the applicability domain to contain other categories of aromatic compounds.

Declaration of Competing Interest

The authors declare that they have no known competing financial interests or personal relationships that could have appeared to influence the work reported in this paper.

Acknowledgements

Financial supports from the National Natural Science Foundation of China (no. 21876108), the NSF ERC on Nanotechnology-Enabled Water Treatment (no. EEC-1449500), and the Special Fund for Agro-Scientific Research in the Public Interest of China (no. 201503107) are gratefully acknowledged.

Appendix A. Supplementary data

Supplementary data to this article can be found online at https://doi.org/10.1016/j.cej.2019.123923.

References

[1] X. Duan, H. Sun, Z. Shao, S. Wang, Nonradical reactions in environmental remediation processes: uncertainty and challenges, Appl. Catal. B 224 (2018) 973–982.
[2] X. Duan, H. Sun, S. Wang, Metal-free carbocatalysis in advanced oxidation reactions, Acc. Chem. Res. 51 (2018) 678–687.
[3] A. Helland, P. Wick, A. Koehler, K. Schmid, C. Som, Reviewing the environmental and human health knowledge base of carbon nanotubes, Environ. Health Persp. 115 (2007) 1125–1131.
[4] E.J. Petersen, L. Zhang, N.T. Mattison, D.M.O. Carroll, A.J. Whelton, N. Uddin, T. Nguyen, Q. Huang, T.B. Henry, R.D. Holbrook, K.L. Chen, Potential release pathways, environmental fate, and ecological risks of carbon nanotubes, Environ. Sci. Technol. 45 (2011) 9837–9856.
[5] J.R. Lead, G.E. Batley, P.J.J. Alvarez, M. Croteau, R.D. Handy, M.J. McLaughlin, J.D. Judy, K. Schirmer, Nanomaterials in the environment: behavior, fate, bioavailability, and effects – an updated review, Environ. Toxicol. Chem. 37 (2018) 2029–2063.
[6] M.S. Mauter, I. Zucker, F. Perreault, J.R. Werber, J. Kim, M. Elimelech, The role of nanotechnology in tackling global water challenges, Nat. Sustain. 1 (2018) 166–175.
[7] H. Sun, S. Liu, G. Zhou, H.M. Ang, M.O. Tad, S. Wang, Reduced graphene oxide for catalytic oxidation of aqueous organic pollutants, ACS Appl. Mater. Interfaces 4 (2012) 5466–5471.
[8] H. Sun, C. Kwan, A. Suvorova, H.M. Ang, M.O. Tad, S. Wang, Catalytic oxidation of organic pollutants on pristine and surface nitrogen-modified carbon nanotubes with sulfate radicals, Appl. Catal. B 154 (2014) 134–141.
[9] X. Duan, Z. Ao, H. Zhang, M. Saunders, H. Sun, Z. Shao, S. Wang, Nanodiamonds in sp^2/ sp^3 configuration for radical to nonradical oxidation: Core-shell layer dependence, Appl. Catal. B 222 (2018) 176–181.
[10] J. Zhang, X. Shao, C. Shi, S. Yang, Decolorization of Acid Orange 7 with peroxymonosulfate oxidation catalyzed by granular activated carbon, Chem. Eng. J. 232 (2013) 259–265.
[11] X. Duan, Z. Ao, L. Zhou, H. Sun, G. Wang, S. Wang, Occurrence of radical and nonradical pathways from carbocatalysts for aqueous and nonaqueous catalytic oxidation, Appl. Catal. B 188 (2016) 98–105.
[12] P. Hu, H. Su, Z. Chen, C. Yu, Q. Li, B. Zhou, P.J.J. Alvarez, M. Long, Selective degradation of organic pollutants using an efficient metal-free catalyst derived from carbonized polypyrrole via peroxymonosulfate activation, Environ. Sci. Technol. 51 (2017) 11288–11296.
[13] X. Chen, W. Oh, T. Lim, Graphene- and CNTs-based carbocatalysts in persulfates activation: material design and catalytic mechanisms, Chem. Eng. J. 354 (2018) 941–976.
[14] X. Duan, H. Sun, Y. Wang, J. Kang, S. Wang, N-doping-induced nonradical reaction on single-walled carbon nanotubes for catalytic phenol oxidation, ACS Catal. 5 (2015) 553–559.
[15] H. Lee, H. Lee, J. Jeong, J. Lee, N. Park, C. Lee, Activation of persulfates by carbon nanotubes: oxidation of organic compounds by nonradical mechanism, Chem. Eng. J. 266 (2015) 28–33.
[16] C. Guan, J. Jiang, C. Luo, S. Pang, C. Jiang, J. Ma, Y. Jin, J. Li, Transformation of iodide by carbon nanotube activated peroxydisulfate and formation of iodoorganic compounds in the presence of natural organic matter, Environ. Sci. Technol. 51 (2017) 479–487.
[17] C. Guan, J. Jiang, S. Pang, C. Luo, J. Ma, Y. Zhou, Y. Yang, Oxidation kinetics of bromophenols by nonradical activation of peroxydisulfate in the presence of carbon nanotube and formation of brominated polymeric products, Environ. Sci. Technol. 51 (2017) 10718–10728.
[18] E. Yun, H. Yoo, H. Bae, H. Kim, J. Lee, Exploring the role of persulfate in the activation process: radical precursor versus electron acceptor, Environ. Sci. Technol. 51 (2017) 10090–10099.
[19] E. Yun, J.H. Lee, J. Kim, H. Park, J. Lee, Identifying the nonradical mechanism in the peroxymonosulfate activation process: singlet oxygenation versus mediated electron transfer, Environ. Sci. Technol. 52 (2018) 7032–7042.
[20] X. Cheng, H. Guo, Y. Zhang, X. Wu, Y. Liu, Non-photochemical production of singlet oxygen via activation of persulfate by carbon nanotubes, Water Res. 113 (2017) 80–88.
[21] Y. Lee, U. von Gunten, Quantitative structure-activity relationships (QSARs) for the transformation of organic micropollutants during oxidative water treatment, Water Res. 46 (2012) 6177–6195.
[22] R. Xiao, T. Ye, Z. Wei, S. Luo, Z. Yang, R. Spinney, Quantitative structure-activity relationship (QSAR) for the oxidation of trace organic contaminants by sulfate radical, Environ. Sci. Technol. 49 (2015) 13394–13402.
[23] T. Ye, Z. Wei, R. Spinney, D.D. Dionysiou, S. Luo, L. Chai, Z. Yang, R. Xiao, Quantitative structure-activity relationship for the apparent rate constants of aromatic contaminants oxidized by ferrate(VI), Chem. Eng. J. 317 (2017) 258–266.
[24] S. Endo, K. Goss, Applications of polyparameter linear free energy relationships in environmental chemistry, Environ. Sci. Technol. 48 (2014) 12477–12491.
[25] O.G. Apul, T. Karanfil, Adsorption of synthetic organic contaminants by carbon nanotubes: a critical review, Water Res. 68 (2015) 34–55.
[26] Y. Wang, J. Chen, X. Wei, A.J. Hernandez Maldonado, Z. Chen, Unveiling adsorption mechanisms of organic pollutants onto carbon nanomaterials by density functional theory computations and linear free energy relationship modeling, Environ. Sci. Technol. 51 (2017) 11820–11828.
[27] J. Brame, M. Long, Q. Li, P. Alvarez, Inhibitory effect of natural organic matter or other background constituents on photocatalytic advanced oxidation processes: mechanistic model development and validation, Water Res. 84 (2015) 362–371.
[28] F.J. Beltrán, F.J. Rivas, R. Montero-de-Espinosa, Iron type catalysts for the ozonation of oxalic acid in water, Water Res. 39 (2005) 3553–3564.
[29] Y. Sugano, M.C. Vestergaard, M. Saito, E. Tamiya, A carbon nanotube structured biomimetic catalyst for polysaccharide degradation, Chem. Commun. 47 (2011) 7176.
[30] H. Wang, P. Li, D. Yu, Y. Zhang, Z. Wang, C. Liu, H. Qiu, Z. Liu, J. Ren, X. Qu, Unraveling the enzymatic activity of oxygenated carbon nanotubes and their application in the treatment of bacterial infections, Nano Lett. 18 (2018) 3344–3351.
[31] J. Hou, H. Li, Y. Tang, J. Sun, H. Fu, X. Qu, Z. Xu, D. Yin, S. Zheng, Supported N-doped carbon quantum dots as the highly effective peroxydisulfate catalysts for bisphenol F degradation, Appl. Catal. B 238 (2018) 225–235.
[32] Y. Ling, M.J. Klemes, S. Steinschneider, W.R. Dichtel, D.E. Helbling, QSARs to predict adsorption affinity of organic micropollutants for activated carbon and β-cyclodextrin polymer adsorbents, Water Res. 154 (2019) 217–226.
[33] M.T. Pérez-Prior, R. Gómez-Bombarelli, M.I. González-Sánchez, E. Valero, Biocatalytic oxidation of phenolic compounds by bovine methemoglobin in the presence of H_2O_2: quantitative structure-activity relationships, J. Hazard. Mater. 241–242 (2012) 207–215.
[34] A.J. Salter-Blanc, E.J. Bylaska, M.A. Lyon, S.C. Ness, P.G. Tratnyek, Structure-activity relationships for rates of aromatic amine oxidation by manganese dioxide, Environ. Sci. Technol. 50 (2016) 5094–5102.
[35] H. Su, C. Yu, Y. Zhou, L. Gong, Q. Li, P.J.J. Alvarez, M. Long, Quantitative structure-activity relationship for the oxidation of aromatic organic contaminants in water by TAML/H_2O_2, Water Res. 140 (2018) 354–363.
[36] J.W. Ponder, TINKER: Software Tools for Molecular Design, 2004, https://dasher.wustl.edu/tinker/.

[37] T.N.G. Borhani, M. Saniedanesh, M. Bagheri, J.S. Lim, QSPR prediction of the hydroxyl radical rate constant of water contaminants, Water Res. 98 (2016) 344–353.
[38] S. Luo, Z. Wei, D.D. Dionysiou, R. Spinney, W. Hu, L. Chai, Z. Yang, T. Ye, R. Xiao, Mechanistic insight into reactivity of sulfate radical with aromatic contaminants through single-electron transfer pathway, Chem. Eng. J. 327 (2017) 1056–1065.
[39] S. Luo, Z. Wei, R. Spinney, F.A. Villamena, D.D. Dionysiou, D. Chen, C. Tang, L. Chai, R. Xiao, Quantitative structure-activity relationships for reactivities of sulfate and hydroxyl radicals with aromatic contaminants through single-electron transfer pathway, J. Hazard. Mater. 344 (2018) 1165–1173.
[40] Y. Zhao, D.G. Truhlar, The M06 suite of density functionals for main group thermochemistry, thermochemical kinetics, noncovalent interactions, excited states, and transition elements: two new functionals and systematic testing of four M06-class functionals and 12 other functionals, Theor. Chem. Acc. 120 (2008) 215–241.
[41] A.V. Marenich, C.J. Cramer, D.G. Truhlar, Universal solvation model based on solute electron density and on a continuum model of the solvent defined by the bulk dielectric constant and atomic surface tensions, J. Phys. Chem. B 113 (2009) 6378–6396.
[42] J. Suatoni, R. Snyder, R. Clark, Voltammetric studies of phenol and aniline ring substitution, Anal. Chem. 33 (1961) 1894–1897.
[43] C. Hansch, A. Leo, R.W. Taft, A survey of Hammett substituent constants and resonance and field parameters, Chem. Rev. 91 (1991) 165–195.
[44] M.H. Abraham, Scales of solute hydrogen-bonding: their construction and application to physicochemical and biochemical processes, Chem. Soc. Rev. 22 (1993) 73–83.
[45] T.H. Nguyen, K. Goss, W.P. Ball, Polyparameter linear free energy relationships for estimating the equilibrium partition of organic compounds between water and the natural organic matter in soils and sediments, Environ. Sci. Technol. 39 (2005) 913–924.
[46] T. Hüffer, S. Endo, F. Metzelder, S. Schroth, T.C. Schmidt, Prediction of sorption of aromatic and aliphatic organic compounds by carbon nanotubes using poly-parameter linear free-energy relationships, Water Res. 59 (2014) 295–303.
[47] P. Gramatica, S. Cassani, P.P. Roy, S. Kovarich, C.W. Yap, E. Papa, QSAR modeling is not “push a button and find a correlation”: a case study of toxicity of (benzo-) triazoles on algae, Mol. Inform. 31 (2012) 817–835.
[48] W. Chen, L. Duan, L. Wang, D. Zhu, Adsorption of hydroxyl- and amino-substituted aromatics to carbon nanotubes, Environ. Sci. Technol. 42 (2008) 6862–6868.
[49] K. Yang, W. Wu, Q. Jing, L. Zhu, Aqueous adsorption of aniline, phenol, and their substitutes by multi-walled carbon nanotubes, Environ. Sci. Technol. 42 (2008) 7931–7936.
[50] N. Jaafarzadeh, F. Ghanbari, M. Ahmadi, Catalytic degradation of 2,4-dichlorophenoxyacetic acid (2,4-D) by nano-Fe_2O_3 activated peroxymonosulfate: influential factors and mechanism determination, Chemosphere 169 (2017) 568–576.
[51] Y. Rao, F. Han, Q. Chen, D. Wang, D. Xue, H. Wang, S. Pu, Efficient degradation of diclofenac by $LaFeO_3$-catalyzed peroxymonosulfate oxidation – kinetics and toxicity assessment, Chemosphere 218 (2019) 299–307.
[52] H. Son, J. Im, K. Zoh, A Fenton-like degradation mechanism for 1,4-dioxane using zero-valent iron (Fe^0) and UV light, Water Res. 43 (2009) 1457–1463.
[53] Z. Khuzwayo, E. Chirwa, Modelling and simulation of photocatalytic oxidation mechanism of chlorohalogenated substituted phenols in batch systems: Langmuir-Hinshelwood approach, J. Hazard. Mater. 300 (2015) 459–466.
[54] B. Zhu, T. Lim, J. Feng, Influences of amphiphiles on dechlorination of a trichlorobenzene by nanoscale Pd/Fe: adsorption, reaction kinetics, and interfacial interactions, Environ. Sci. Technol. 42 (2008) 4513–4519.
[55] A. Tropsha, P. Gramatica, V.K. Gombar, The importance of being earnest: validation is the absolute essential for successful application and interpretation of QSPR models, QSAR Combust. Sci. 22 (2003) 69–77.
[56] W. Chen, L. Duan, D. Zhu, Adsorption of polar and nonpolar organic chemicals to carbon nanotubes, Environ. Sci. Technol. 41 (2007) 8295–8300.
[57] S.E. Wheeler, Understanding substituent effects in noncovalent interactions involving aromatic rings, Acc. Chem. Res. 46 (2012) 1029–1038.
[58] K. Yang, B. Xing, Adsorption of organic compounds by carbon nanomaterials in aqueous phase: Polanyi theory and its application, Chem. Rev. 110 (2010) 5989–6008.
[59] X. Xia, N.A. Monteiro-Riviere, J.E. Riviere, An index for characterization of nanomaterials in biological systems, Nat. Nanotechnol. 5 (2010) 671–675.
[60] O.G. Apul, Q. Wang, T. Shao, J.R. Rieck, T. Karanfil, Predictive model development for adsorption of aromatic contaminants by multi-walled carbon nanotubes, Environ. Sci. Technol. 47 (2013) 2295–2303.
[61] Y. Shih, P.M. Gschwend, Evaluating activated carbon-water sorption coefficients of organic compounds using a linear solvation energy relationship approach and sorbate chemical activities, Environ. Sci. Technol. 43 (2009) 851–857.
[62] C.A. Hunter, J.K.M. Sanders, The nature of π-π interactions, J. Am. Chem. Soc. 112 (1990) 5525–5534.
[63] P.G. Tratnyek, J. Hoigne, Oxidation of substituted phenols in the environment: a QSAR analysis of rate constants for reaction with singlet oxygen, Environ. Sci. Technol. 25 (1991) 1596–1604.
[64] J.Y. Hu, T. Morita, Y. Magara, T. Aizawa, Evaluation of reactivity of pesticides with ozone in water using the energies of frontier molecular orbitals, Water Res. 34 (2000) 2215–2222.
[65] S. Gupta, N. Basant, Modeling the aqueous phase reactivity of hydroxyl radical towards diverse organic micropollutants: an aid to water decontamination processes, Chemosphere 185 (2017) 1164–1172.
[66] C. Liers, E. Aranda, E. Strittmatter, K. Piontek, D.A. Plattner, H. Zorn, R. Ullrich, M. Hofrichter, Phenol oxidation by DyP-type peroxidases in comparison to fungal and plant peroxidases, J. Mol. Catal. B 103 (2014) 41–46.
[67] C. Li, S. Zheng, T. Li, J. Chen, J. Zhou, L. Su, Y. Zhang, J.C. Crittenden, S. Zhu, Y. Zhao, Quantitative structure-activity relationship models for predicting reaction rate constants of organic contaminants with hydrated electrons and their mechanistic pathways, Water Res. 151 (2019) 468–477.
[68] X. Wang, Y. Qin, L. Zhu, H. Tang, Nitrogen-doped reduced graphene oxide as a bifunctional material for removing bisphenols: synergistic effect between adsorption and catalysis, Environ. Sci. Technol. 49 (2015) 6855–6864.
[69] S. Zhu, X. Huang, F. Ma, L. Wang, X. Duan, S. Wang, Catalytic removal of aqueous contaminants on N-doped graphitic biochars: inherent roles of adsorption and nonradical mechanisms, Environ. Sci. Technol. 52 (2018) 8649–8658.